Chinese Journal of Aeronautics, (2017), 30(5): 1631–1643

Chinese Society of Aeronautics and Astronautics
& Beihang University

Chinese Journal of Aeronautics

cja@buaa.edu.cn
www.sciencedirect.com

# Effect of an end plate on surface pressure distributions of two swept wings

**Mohammad Reza SOLTANI** [a], **Mehran MASDARI** [b,*], **Mohammad Rasoul TIRANDAZ** [a]

[a] *Department of Aerospace Engineering, Sharif University of Technology, Tehran 19166, Iran*
[b] *Faculty of New Sciences and Technologies, University of Tehran, Tehran, Iran*

Received 19 July 2016; revised 19 December 2016; accepted 24 January 2017
Available online 22 August 2017

**KEYWORDS**

Chordwise;
Flow field;
Pressure distribution;
Swept wing;
Wind tunnel

**Abstract** A series of wind tunnel tests was conducted to examine how an end plate affects the pressure distributions of two wings with leading edge (LE) sweep angles of 23° and 40°. All the experiments were carried out at a midchord Reynolds number of $8 \times 10^5$, covering an angle of attack (AOA) range from −2° to 14°. Static pressure distribution measurements were acquired over the upper surfaces of the wings along three chordwise rows and one spanwise direction at the wing quarter-chord line. The results of the tests confirm that at a particular AOA, increasing the sweep angle causes a noticeable decrease in the upper-surface suction pressure. Furthermore, as the sweep angle increases, the development of a laminar separation bubble near the LEs of the wings takes place at higher AOAs. On the other hand, spanwise pressure measurements show that increasing the wing sweep angle results in forming a stronger vortex on the quarter-chord line which has lower sensitivity to AOA variation and remains substantially attached to the wing surface for higher AOAs than that can be achieved in the case of a lower sweep angle. In addition, data obtained indicate that installing an end plate further reinforces the spanwise flow over the wing surface, thus affecting the pressure distribution.



## 1. Introduction

Calculation of pressure distribution over airfoils operating in inviscid flow, is one of the classic problems of the fluid motion theory. Consequently, it has regained significance in designing swept wing aircraft.

The reasons for the application of swept wings to high-subsonic-speed aircraft are now well-established. Namely, a swept wing has a greater critical Mach number than that of a corresponding unswept wing. In addition, the variation of

* Corresponding author.
E-mail address: m.masdari@ut.ac.ir (M. MASDARI).

Peer review under responsibility of Editorial Committee of CJA.

Production and hosting by Elsevier

http://dx.doi.org/10.1016/j.cja.2017.07.008

pressure coefficient with Mach number for a given swept wing is smaller compared to that of an unswept wing with the same airfoil shape. Moreover, on a swept wing, the critical value of pressure coefficient is reached at a higher freestream Mach number. Furthermore, at low Mach numbers, the perturbation velocities are small compared with those of an unswept wing.

The tendency of a sweptback wing to tip stall is due to the induced spanwise flow of the boundary layer from root to tip. Since the tip of a sweptback wing is located aft part of the wing (behind the center of lift), it has the effect of moving the center of lift forward, causing a sharp pitch-up movement and thus making the stall worse than it was. The tendency to tip stall is the greatest when wing sweep and taper are combined.

There are many studies containing experimental pressure distribution measurements. For example, in 1952, a series of low-speed wind tunnel tests was conducted to determine boundary layer and surface pressure distribution characteristics of a family of sweptback wings. As a result, it was found that the experimental data would have had application in giving a better understanding of the viscous flow phenomena on sweptback wings, particularly in relation to the stall phenomena.[1] Likewise, in 1964, an experimental study was conducted on sweptback wings at the Ames Research Center to investigate the stall characteristics of swept wings.[2] In addition, in 1990, a comprehensive experimental study at the NASA Langley Research Center was conducted on F-14A variable swept wings modified for laminar flow, to assess the transition location under various conditions. Accordingly, left- and right-wing pressure distribution measurements at various Mach numbers and two different altitudes were used to give an explanation for the increased response amplitude of the right wing.[3] Furthermore, in 1997, a detailed investigation was conducted on F-111 aircraft modified with a variable-sweep supercritical mission adaptive wing (MAW) at the Dryden Flight Research Center, to improve the aerodynamic characteristics.[4] Moreover, in 2011, a series of experimental studies was conducted to examine the flow field over a swept wing under various conditions at Sharif University of Technology. Subsequently, measurements of pressure distribution were used to predict the transition point at each chordwise section.[5] Further, surface pressure distribution over a swept wing was exerted by Yen and Hsu[6] to investigate the effects of angle of attack $\alpha$ and chord Reynolds number $Re_c$ on vortex shedding and aerodynamic coefficients.

On all subsonic wings there is a tendency for a secondary flow to develop from the high-pressure region below the wing round the wingtip to the relatively low-pressure region on the upper surface.[7] At a positive lift condition, the flow close to the tip of a three-dimensional wing tends to curl around the tip, because the flow is forced from the lower surface region (high-pressure side) to the upper surface region (low-pressure side) in a circular fashion (Fig. 1). This tendency for the flow to leak around the tip causes a circular three-dimensional flow pattern named vortex, which features a low-pressure core. Viewed from behind, the port wing tip vortex rotates clockwise and the starboard vortex rotates counterclockwise. Aircraft that encounter the wing tip vortices of large preceding aircraft can experience severe upward or downward loads as well as an overpowering rolling moment.

The research on the wing tip vortices began in the fifties and it is still an ongoing study because of its wide range of applications and because of the big number of fluid dynamic features

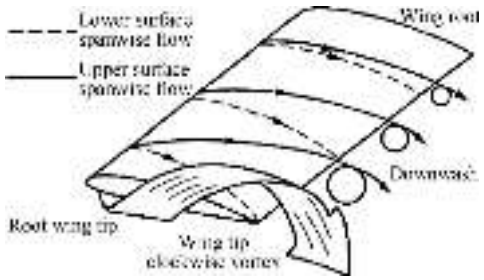


**Fig. 1** Wing tip vortex.

that it implies: vorticity sheet rolling up, multiple vortex system, high turbulence level and relaminarization, diffusion, decay, collapse, instability and merging of vortices are just a few numbers of the aspects that coexist in this phenomena.[8]

Significant efforts have been utilized to investigate the formation and decay process of a wing tip vortex. Some of those efforts have been summarized by Spalart.[9] Winglets, end plates, tip sails, wing-grids, and blowing jets are typical examples of mechanisms for wing tip vortex control. They are effective in decreasing the strength of the trailing wing tip vortex and reducing the induced drag.[10]

The effect of eliminating wing tip vortices on aerodynamic characteristics has not been fully investigated until now. Only few experimental investigations on the effect of an end plate were conducted by Fink and Lastinger[11] and Carter.[12] Fink and Lastinger performed a series of wind-tunnel investigations to determine the ground effect on the aerodynamic characteristics of thick and highly cambered wings with various aspect ratios. Further, in 2008, a numerical analysis was performed to investigate the aerodynamic characteristics and static height stability of an end plate on an aspect-ratio-one wing in ground effect.[13]

End plates are commonly installed on aerodynamic models to mitigate three-dimensional end effects. Furthermore, experimental studies on flow development over non-circular geometries have similarly found that improved mean spanwise uniformity can be achieved by installing end plates on these models.[14] Moreover, end plates have been used in a number of experimental studies on airfoils operating at low Reynolds numbers.[15–18]

It should further be noted that a preceding work done by Soltani et al.[19] has successfully investigated the influence of Reynolds number on the surface pressure distribution over the same wing models without an end plate. In addition, Pelletier and Mueller[18] investigated the effects of end plates on force balance measurements for a two-dimensional Eppler 61 airfoil model at chord Reynolds numbers between $40 \times 10^3$ and $100 \times 10^3$. As a result, they demonstrated that the presence of end plates has a strong effect on lift and drag coefficients at low Reynolds numbers.

The purpose of this investigation is to assess the effects of end plates on the surface pressure distributions of two sweptback wings. Static pressure distributions along three chordwise rows and similar pressure measurements along one spanwise direction are obtained at a midchord Reynolds number of $0.8 \times 10^5$ and at angles of attack (AOAs) ranging from $\alpha = -2^\circ$ to $\alpha = 14^\circ$.

## 2. Experimental apparatus

All experiments were conducted in a closed-loop subsonic wind tunnel with a test section size of 80 cm × 80 cm × 200 cm in height, width, and depth, respectively. The tunnel can be operated over a speed range of 10–100 m/s. The free-stream velocity $V_\infty$ was measured using a pitot-static tube. Flow conditioning was accomplished by a section of four large, anti-turbulence screens and aluminum honeycomb installed upstream at a 7:1 contraction section, producing a freestream turbulence intensity of less than 0.1%. In addition, the non-uniformity of the average velocity across the cross-section was less than 0.5 percent.

In this investigation, two semi-span 1 : 2.5 scaled models, which are made of aluminum alloy, were used as test cases for which the effects of experimental setup on surface pressure distribution were evaluated. The wing models, which have airfoil sections similar to that of NACA 6-series, have a leading edge sweep $\Lambda$ of 23° and 40°. Furthermore, the root chord length $C_r$ is 394 mm, the tip chord length $C_t$ is 172 mm, and the wing semi span ($b/2$) is 516 mm, which yield a semi-span aspect ratio of 0.43 (Fig. 2). A polished aluminum alloy plate with a rounded leading edge (LE) and trailing edge (TE) was installed over the test section floor to decrease the boundary layer effect of the test section on the model. In addition, to eliminate the formation of wing tip vortices, a Plexiglas flat plate with a rounded LE and TE and a size of 100 cm × 100 cm × 1 cm in width, length, and height respectively, was installed on the tip of a wing. The wing models were mounted on a support and then inserted through a boundary-layer thickness controlling plate. In Fig. 2(a), the general arrangement of each model used for this investigation when installed in the wind tunnel is illustrated.

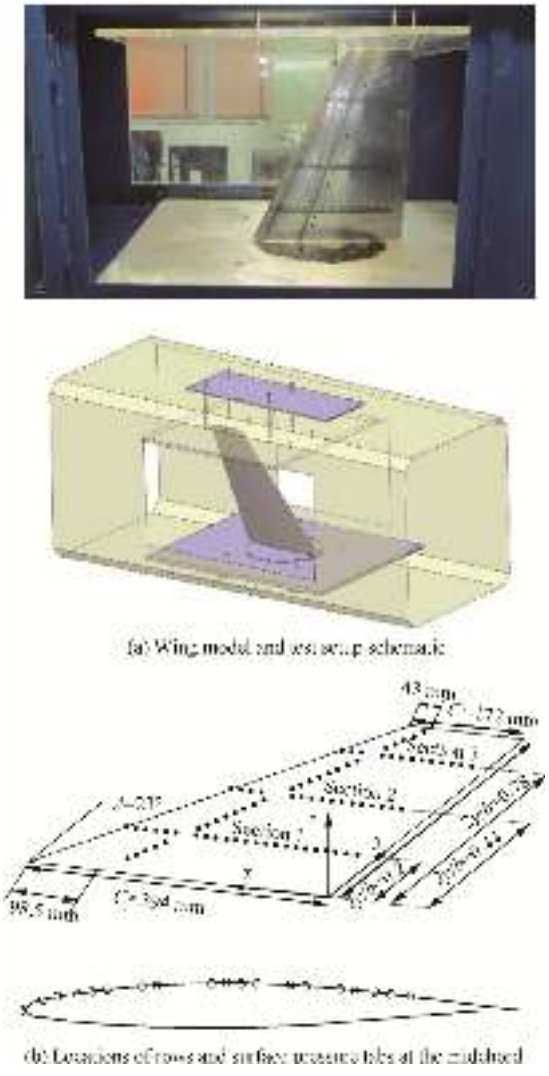

**Fig. 2** Wing model and test setup schematic, and locations of rows and surface pressure tabs at the midchord.

In this study, a pressure instrumentation was located on the right-wing model of the real airplane. A total of ninety static pressure taps of 0.4 mm in diameter were distributed along the model surface in three chordwise rows, i.e., the inboard station of the wing (Section 1, $2y/b = 0.2$), the middle station (Section 2, $2y/b = 0.44$), and the outboard station (Section 3, $2y/b = 0.78$), as well as in one spanwise row along the quarter-chord line (Fig. 2(b)).

The pressure taps distributed on the upper surface of the wing were connected by stainless steel tubing to accurate pressure transducers. In most cases, the lengths of the pressure lines from the orifices to the transducers were limited to less than 1.5 m, thus minimizing pressure lag effects. Furthermore, each transducer's data were collected via a terminal board and transformed to a computer through a 64-channel, 12-bit analog-to-digital (A/D) board capable of an acquisition rate of up to 500 kHz. The raw data were then digitally filtered using a low-pass filtering routine. During the filtering process, the cutoff frequency was calculated from either the power spectrum estimation or frequency-domain analysis. The advantage of this method is that the noise, which may dominate the signal in the time domain, appears only as a single peak or spike in the frequency-domain.[20]

## 3. Presentation of results

Static pressure distributions over the upper surfaces of the wings, in both chordwise and spanwise directions, were measured at different angles of attack. Chordwise pressure data will be presented first, followed by those of spanwise measurements, and finally a comparison between the measurements obtained in this experiment (wing with an end plate, WWE) and the results of the case without an end plate (WOE) will be given. Each figure of the pressure plots is associated with a sketch to illustrate the sweep angles of the wings and the relative locations of the rows of pressure taps.

### 3.1. Chordwise pressure distribution results

#### 3.1.1. Effect of angle of attack on chordwise $C_p$

Middle-section static pressure coefficient $C_p$ distributions for angles of attack from −2° to 6° are presented in Fig. 3 for both wing models. As illustrated in this figure, at low AOAs, $-2° \leqslant \alpha \leqslant 2°$, the wing section airfoil has a thickness distribution that leads to a favorable pressure gradient over a large part of the airfoil. Furthermore, over a significant part of the wing chordwise Section, the flow is attached to the surface. It should further be noted that in the region over the wing sur-

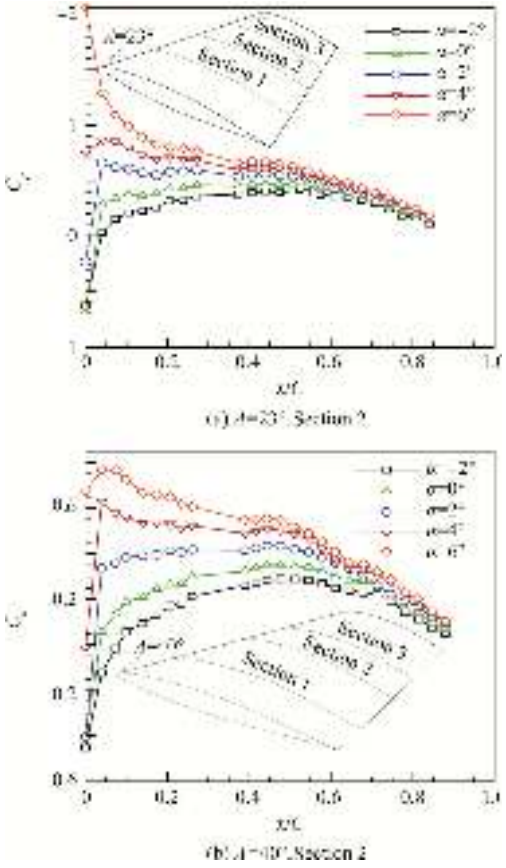

**Fig. 3** Effect of AOA on $C_p$ over the middle section, for $-2^\circ \leqslant \alpha \leqslant 6^\circ$.

face where $dC_p/dx < 0$, called favorable pressure gradient region, the value of $C_p$ increases negatively, creating a stronger suction force over the wing surface; conversely in the region over the wing surface where $dC_p/dx > 0$, called adverse pressure gradient, the magnitude of $C_p$ decreases, but the value of $C_p$ increases positively.

As the AOA increases, a suction peak in the chordwise pressure distribution can be seen that moves upstream (Fig. 3). For example, on Section 2 of the 40°-sweep (40DS) wing, at an angle of attack of 0°, the pressure peak is detected at $x/C \cong 0.47$, $C$ is airfoil chord, but as the angle of attack increases to 2° and 4°, the point of $C_{p,\min}$ moves to $x/C \cong 0.44$ and $x/C \cong 0.03$, respectively (Fig. 3(b)). The increment of the suction peak, which is an indication of increasing the speed of the air moving past the wing and generating stronger suction pressure on its surface, is clearly visible when increasing the angle of attack (Fig. 3).

The results show that when the 23°-sweep (23DS) wing is at angles of attack greater than 4°, the adverse pressure gradient aft of the point of the suction peak on the middle station becomes stronger (Figs. 3(a) and 4). A high suction peak near the wing leading edge indicates that the flow becomes turbulent close to the leading edge where $x/C > 0$. Static surface pressure measurements demonstrate that for angles of attack of 6° and 8°, the flow will definitely become turbulent in a region of $0 \leqslant x/C \leqslant 0.17$. On the contrary, the flow over the wing surface of this station (Section 2) seems to be completely

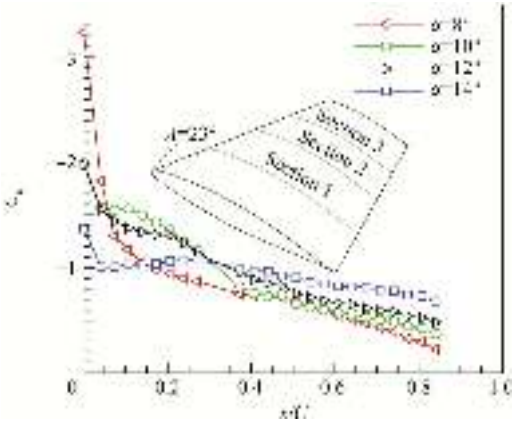

**Fig. 4** Effect of AOA on $C_p$ over the middle section, for $\Lambda = 23^\circ$ and $8^\circ \leqslant \alpha \leqslant 14^\circ$.

attached for an angle of attack range of $-2^\circ \leqslant \alpha \leqslant 8^\circ$. It should be pointed out that due to practical reasons, no pressure tap was installed at $x/C > 0.8$; therefore, results could not be obtained close to the wing trailing edge (Fig. 2(b)).

With an increasing angle of attack to 10°, the pressure distribution over the surface of the 23DS wing represents a significant decrease in the magnitude of $C_{p_{,\min}}$ and a slight peak at the LE, $x/C = 0$, followed by a region of relatively constant pressure from $x/C = 0.04$ aft to $x/C = 0.1$, and a lack of complete pressure recovery near the TE of the wing (Fig. 4). The plateau of the pressure distribution is a characteristic of a laminar separation bubble.[21]

For Reynolds numbers from about $0.8 \times 10^6$ to $1.2 \times 10^6$, laminar separation on an airfoil occurs when an adverse pressure gradient of sufficient strength is imposed on an approaching laminar boundary layer and the flow near the surface is forced to zero velocity at the point of separation. When sufficient pressure recovery is achieved with some distance downstream, the flow reattaches, forming a separation bubble. Furthermore, flow separation leads to the formation of a shear layer, which divides the recirculating flow within the bubble and the external freestream flow. Before the laminar shear layer transits to turbulent flow, the static pressure in the bubble remains fairly constant, and the speed of the reverse flow is very slow. The beginning and end of this pressure plateau, which is commonly termed as the "dead-air" region, mark the locations of laminar boundary layer separation and separated shear layer transition, respectively. Entrainment of high-energy external flow by the turbulent shear layer allows for adequate pressure recovery and results in flow reattachment.[22]

Considering the data obtained in this investigation, local separation of the flow first appears near the wing LE, followed by reattachment of the flow farther aft and then recovery to essentially freestream pressure. From Fig. 4, it can be seen that with an increasing angle of attack from 8° to 14°, the suction peak value continues to increase from −3.23 to −1.37, $|C_p|$ increases near the TE from 0.22 to 0.67, the pressure plateau lengthens from $0.04 \leqslant x/C \leqslant 0.1$ for $\alpha = 10^\circ$ to $0.04 \leqslant x/C \leqslant 0.27$ for $\alpha = 14^\circ$, and the point of reattachment moves downstream from $x/C = 0.1$ to $x/C = 0.27$.

*3.1.2. Effect of spanwise location on chordwise $C_p$*

Fig. 5 shows a comparison between the measured pressure distributions at three spanwise locations of the 23DS wing for angles of attack of 0°, 8°, 10°, 12°, and 14°. From the data obtained, a slight amount of longitudinal shift in the pressure peak can be detected, as the distance from the wing root to the wing tip is increased (Fig. 5(a)).

The pressure distribution measurements show a sudden drop in the magnitude of $C_p$ near the TE of Section 3 for the 23DS wing (Fig. 5(a)). Moreover, the data obtained indicate that with an increasing angle of attack, $|C_p|$ drops more sharply in this area of the wing surface (Fig. 5(a)–(e). As will be discussed in Section 3.3 of this article, with an increasing AOA, a vortex-shaped flow forms on the surface of the end

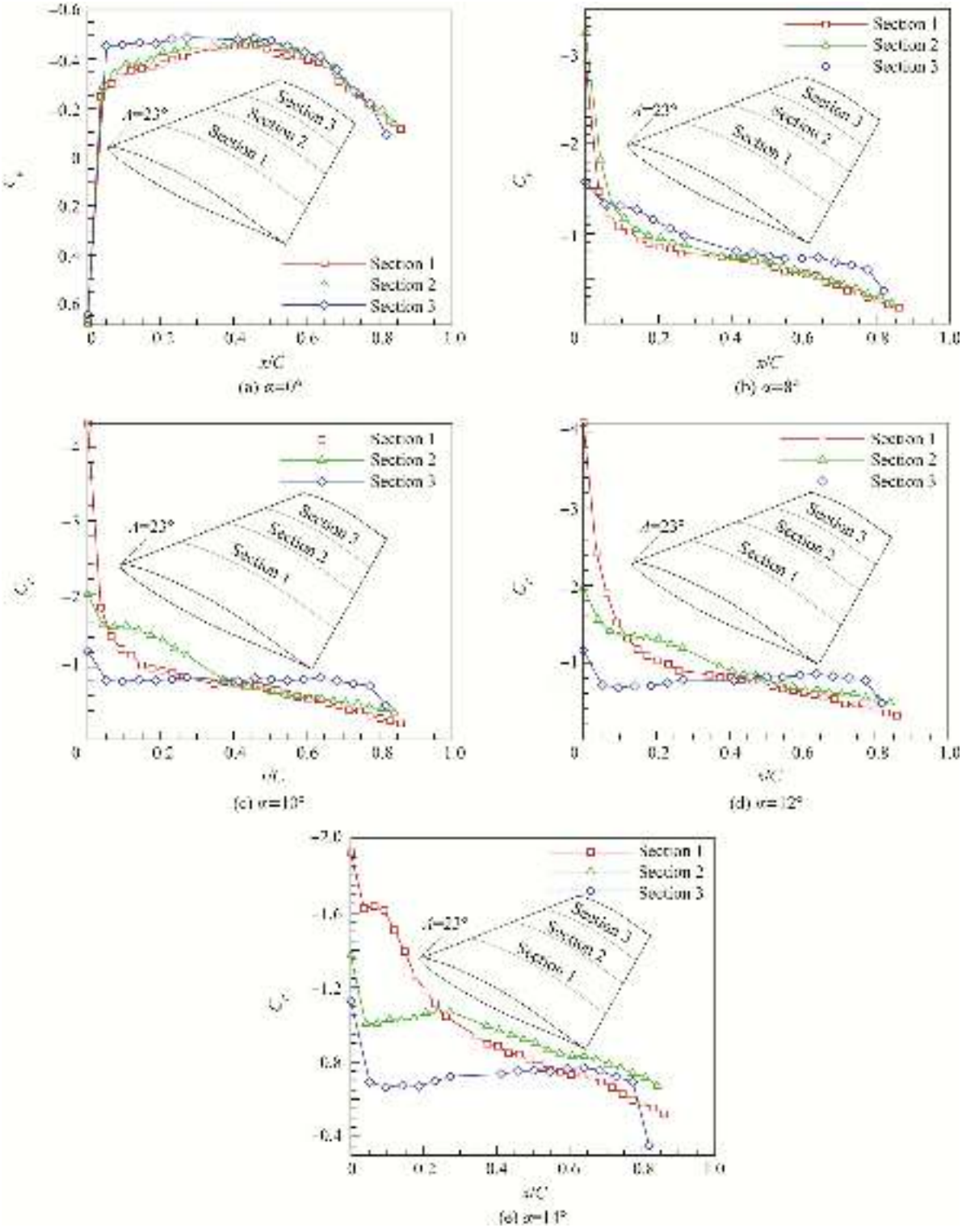


**Fig. 5** Effect of spanwise location on chordwise pressure distribution for $\Lambda = 23°$.

plate, to which an increasing angle of attack causes its size and strength to increase, thus affecting a larger area of the flow field near the tip of the wing surface and resulting in a stronger spanwise flow. As a result, this vortex affects the airstream velocity along the outboard section near the TE, and causes a sudden drop in the pressure distribution near the trailing edge of the outboard Section.

From Fig. 5(b), it can be noted that when the 23DS wing is at an 8° angle of attack, at a location downstream from the suction peak, the rate of pressure recovery on Section 3 decreases significantly, creating a pressure plateau in the pressure distribution. As it was previously mentioned, this plateau of the pressure distribution which covers a region of $0.04 < x/C < 0.14$, is an indication of the laminar separation bubble formation. In contrast, there is no indication of local separation on Sections 1 and 2. As the AOA increases to 10°, the rearward edge of the area of laminar boundary layer separation on the $0.03 \leqslant x/C \leqslant 0.09$ outboard station moves toward the trailing edge of the wing, and the enclosed separation bubble increases in size, becoming quite apparent before the separation spreads to the TE (Fig. 5(c)). At this point, the separation bubble cannot recover the pressure and separates from the wing surface, which results in complete Sectional separation over the entire chord length; while in the middle-Section pressure distribution, just a local separation near the LE can be observed, which covers a region of $0.04 \leqslant x/C \leqslant 0.1$, and is followed by reattachment of the flow farther aft. Furthermore, over the inboard Section, the flow is attached to the surface and no characteristic of a stalled airfoil or local separation exists.

As the angle of attack increases to 1°, the length of the area of constant pressure on Section 2 increases in size and covers a region of $0.07 \leqslant x/C \leqslant 0.2$. At the same time, increasing the minimum value of the outboard-Section pressure distribution, lack of pressure recovery near the trailing edge, and a constant $C_p$ from $x/C = 0.05$ to $x/C = 0.77$ all indicate complete separation of the flow over the entire chord of Section 3 (Fig. 5(d)). From Fig. 5(e), it can be observed that at a 14° angle of attack, there exists a pressure plateau near the leading edge of Section 1 covering a region of $0.03 \leqslant x/C \leqslant 0.09$. As noted before, this area of constant pressure is a characteristic of a laminar separation bubble which indicates local separation. As the distance from the wing root to the wing tip is increased, the length of the pressure plateau increases in size and covers a region of $0.04 \leqslant x/C \leqslant 0.27$ on the mean aerodynamic chord $\overline{C}$ (Section 2); however, there is some pressure recovery after this area of constant pressure, indicating a tendency toward reattachment of the flow. On Section 3, $C_p$ is nearly constant in a region of $0.05 \leqslant x/C \leqslant 0.77$, indicating that the flow is separated in this region of the wing.

It is thought that this laminar bubble type of separation leads to formation of a continuous vortex streak, which streams inboard and aft when increasing the angle of attack from 8° (initial appearance near the LE of Section 3) to 14° (initial appearance near the LE of Section 1). When the 23°-sweep wing is at a 14° angle of attack, a spreading-out of the separation streak over a larger chordwise distance can be noted as the distance from the origin of the streak is increased (Fig. 5(e). It may be that the complete separation noted above is the result of this spreading-out process. On the other hand, with respect to, Ref.[23] because of the usual sectional lift coefficient distribution on a swept wing, the bubble appears first at the tip (for an angle of attack of 8°, Fig. 5 (b)) and spreads slowly toward the root, as the wing angle of attack is increased (comparing Fig. 5(b)–(e)). In this case, before the leading-edge bubble spreads to the root, the section near the wing tip (Section 3) has complete separation, and the bubble has curved back to leave the wing at the farthest inboard point where separation has reached the trailing edge (Fig. 5(e). As the angle of attack is increased, both the origin of the bubble and the point at which it leaves the wing move inboard (Fig. 5(b)–(e)).

#### 3.1.3. *Effect of increasing sweep angle on chordwise $C_p$*

Fig. 6 illustrates the chordwise pressure distributions for the two wing models at various angles of attack. In Fig. 6(a), the pressure distributions for the middle station (Section 2) are compared for the two sweep angles at an angle of attack of 2°. It can be seen that as the sweep angle increases, the value of pressure coefficient increases negatively, creating less suction over the wing surface.

Results show that as the sweep angle increases, the formation of a laminar separation bubble takes place at higher angles of attack. Furthermore, with an increasing sweep angle, at a specified angle of attack, the length of the pressure plateau decreases. The results in Fig. 6(b) show that at a 12° angle of attack, there is no indication of local separation or sectional stall in the inboard section pressure distribution, for both sweep angles. As the angle of attack increases to 14°, a pressure plateau close to the LE of the inboard section of the 23DS wing can be seen, which covers a region of $0.03 \leqslant x/C \leqslant 0.09$, while on the inboard station (Section 1) of the 40DS wing, there is no sign of a pressure plateau (Fig. 6(c)). As discussed before, this area of constant pressure is a characteristic of a laminar separation bubble and indicates local separation of the flow.

The formation of a laminar separation bubble near the middle-station LE of the 23DS wing, which covers a region of $0.04 \leqslant x/C \leqslant 0.1$, takes place at an angle of attack of 10°. This constant pressure area is followed by flow reattachment farther aft and recovery to essentially free-stream pressure (Fig. 6(d)). From Fig. 6(d), it can be observed that the laminar separation bubble on the middle station of the 40DS wing is formed at an angle of attack of 10°, covering a region of $0 \leqslant x/C \leqslant 0.03$. It should be noted that, however, the separation bubbles on the middle sections of the two models are detected at the same AOA, and it is seen that as the sweep angle increases, the separation bubble's covering region decreases from $0.041 \leqslant x/C \leqslant 0.1$ in the case of the 23DS wing to $0 \leqslant x/C \leqslant 0.03$ in the case of the 40DS wing. Moreover, Fig. 6(d) shows that with an increasing sweep angle, the slope of the pressure recovery aft of the separation bubble increases. Pressure measurements show that as the angle of attack increases, the lengths of the laminar separation bubbles on Section 2 of the models increase in size, but in the range of angle of attack under experiments, there is no sign of complete flow separation over the entire chord of Section 2 (Fig. 6(e) and (f)).

The separation bubble in the outboard section pressure distribution of the 23DS wing is observed at an angle of attack of 8° (Fig. 6(g)), which covers a region of $0.05 < x/C < 0.14$; while on the 40DS wing's outboard section, laminar boundary

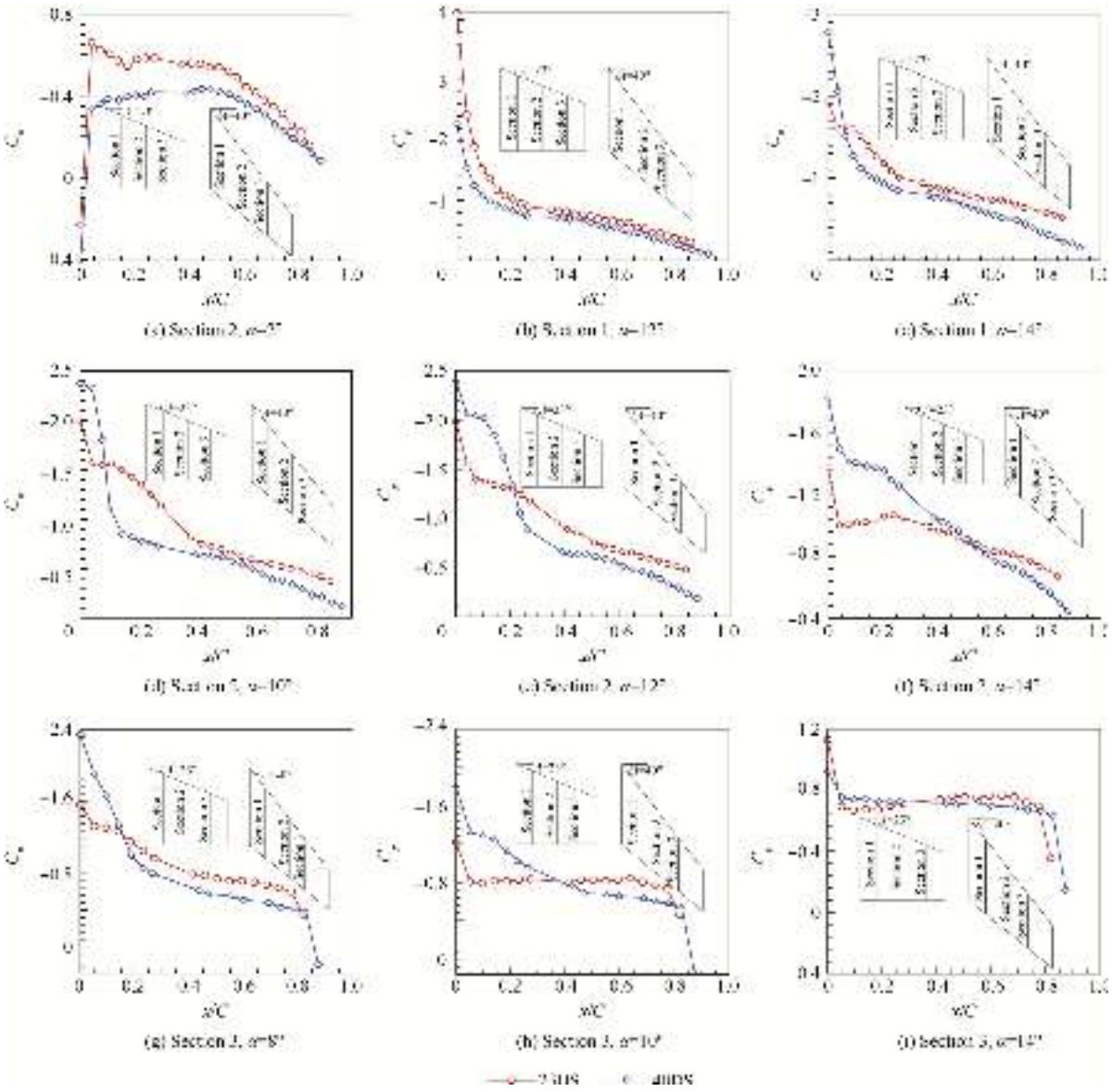

**Fig. 6** Effect of sweep angle on chordwise pressure distributions of wing models at various AOAs.

layer separation is seen at an angle of attack of 10°, which covers an area of $0.05 < x/C < 0.14$ (Fig. 6(h)). Moreover, pressure distribution results show that the magnitude of pressure coefficient near the trailing edge of section 3 drops more sharply, with an increasing sweep angle. As mentioned before, the vortex-shaped flow formed on the surface of the end plate results in a spanwise flow from the tip to the root and in the opposite direction of the swept wing spanwise flow, thereby affecting the airstream velocity along the outboard section near the trailing edge and causing a sudden drop in the pressure distribution near the trailing edge of the outboard station (Section 3). It seems that with an increasing sweep angle, the vortex formed on the surface of the end plate gets stronger, further affecting the velocity of streamwise flow near the trailing edge of the outboard station.

It can be noted that at a 10° angle of attack, there is an indication of separation over the entire chord length on the outboard station of the 23DS wing (Fig. 6(h)), while in the outboard section pressure distribution of the 40DS wing, characteristics of a stalled airfoil can be seen at an AOA of 14° (Fig. 6(i)).

As illustrated in Fig. 6, at a particular angle of attack, the lengths of the laminar separation bubbles over the two wings' chordwise sections decrease with an increasing sweep angle. Furthermore, increasing the sweep angle causes the stall phenomena on the chordwise sections to delay. It can be seen that at an angle of attack of 10°, the flow over the outboard section of the 23DS wing is completely separated, and characteristics of a stalled airfoil are clearly visible; nevertheless, over the outboard section of the 40DS wing, the pressure measurements show a localized separation which covers a region of $0.05 < x/C < 0.14$ followed by reattachment of the flow. Furthermore, no characteristic of a stalled airfoil can be observed, and the air flow is not separated completely (Fig. 6(h)).

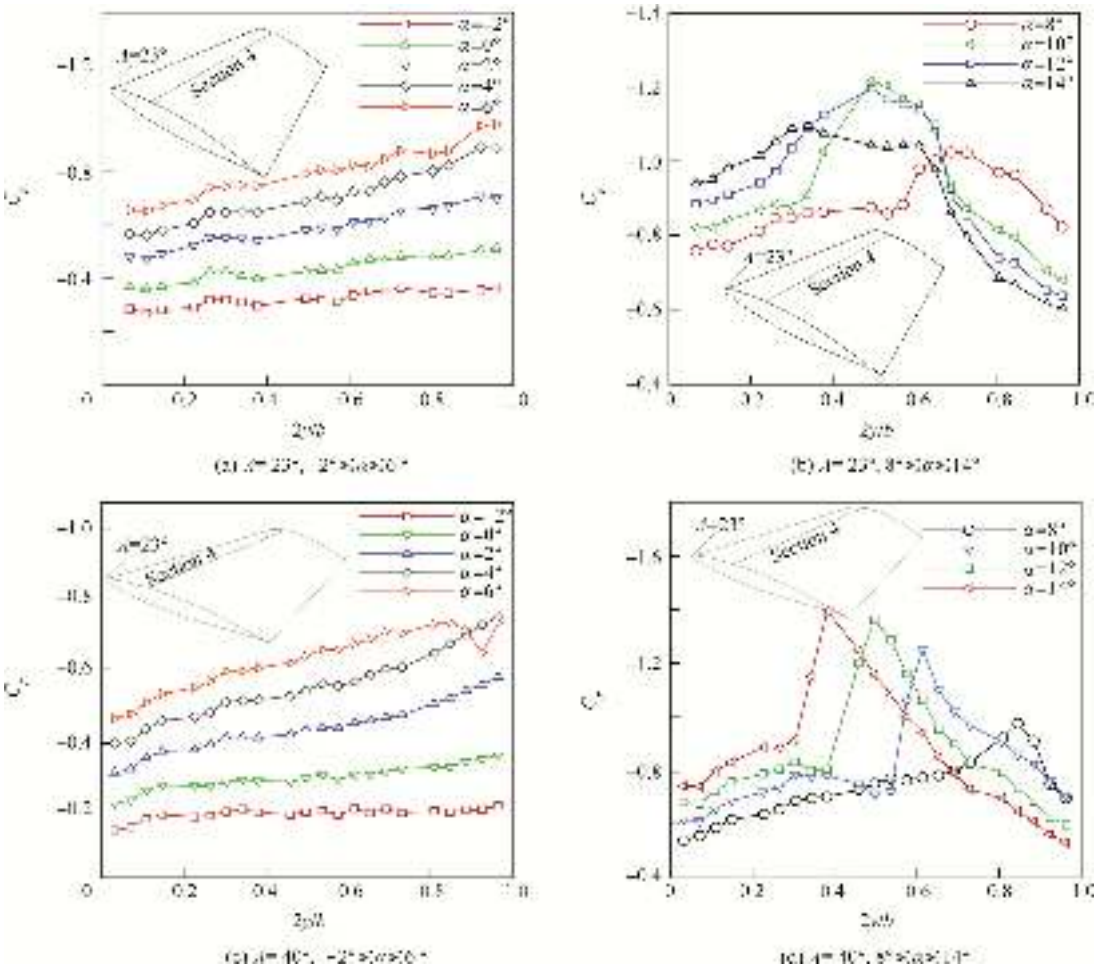

**Fig. 7** Spanwise pressure distribution along quarter-chord line.

### 3.2. Spanwise pressure distribution results

#### 3.2.1. Effect of angle of attack on spanwise $C_p$

Fig. 7(a) and (b) shows the measured spanwise pressure distributions in terms of $C_p$ versus $2y/b$ along the quarter-chord lines of the models at angles of attack ranging from $-2°$ to 14°. As illustrated in Fig. 7(a) and (b), for low angles of attack, the values of $C_p$ slightly decrease along the span from the wing root to the wing tip, which indicate a stronger suction force dominating the outboard region of the wing. It is found that the magnitudes of pressure coefficients are the lowest near the wing root and increase outboard, which of course is a characteristic of swept wings. Furthermore, from the pressure results, it can be seen that with an increasing AOA from $-2°$ to 4°, the slope of the pressure distribution increases, which suggests that the suction pressure near the wing tip is getting stronger more rapidly, compared to that of the inboard region of the wing. The rate of change of the $C_p$ curve slope for AOAs ranging from $-2°$ to 4° is presented in Fig. 8 for both wing models.

The results obtained suggest that at a specific AOA, a distortion in the pressure distribution near the wing tip area can be seen. Furthermore, with an increasing angle of attack, a large portion of the spanwise section near the wing tip is dominated by a very-low-pressure area. Generally, the distortion

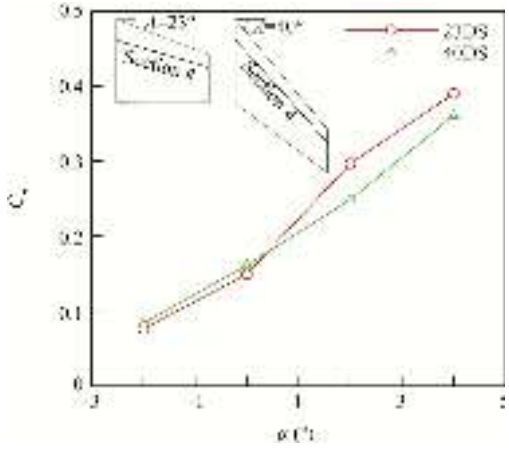

**Fig. 8** Variation of spanwise pressure distribution curve slope.

observed in this area, which is due to the formation of a vortex, and the low pressure associated with the centrifugal force caused by this vortex lead to the formation of a lower-pressure area on the wing surface (Fig. 7(b) and (d)).

Spanwise pressure results show that this vortex due to the sweep angle, forms near the tip of the 23DS wing at an 8° AOA, covering an area of $0.54 < 2y/b < 0.97$ (Fig. 7(b)). As

it is shown in Fig. 7(b), the point of the minimum pressure, which shows the vortex core location, pushes inward from the wing tip to the wing root, increasing the covered area over the quarter-chord line, when increasing the AOA. At a 12° angle of attack, a slight drop in the minimum value of the pressure coefficient suggests that the core of the vortex just starts to get farther from the surface. In addition, it can be easily seen that with increasing the AOA to 14°, the strength of the vortex decreases significantly and the pressure peak drops from −1.21 to −1.19, due to a greater distance between the vortex core and the wing surface. Moreover, it is found that as the AOA increases from 8° to 10°, a sudden drop in the spanwise $C_p$ near the tip of the wing indicates that this region of the wing is experiencing an incipient stall due to the vortex breakdown. In addition, the results show that the separation area moves from the wing tip to the wing root, when increasing the angle of attack from 8° to 14°.

In the case of the 40DS wing, the distortion observed in the pressure distribution, which leads to forming a low-pressure area near the wing tip, is seen at an angle of attack of 6°. Like the case of the 23DS wing, as the AOA gets higher, the vortex increases in size and gets stronger, further reducing the pressure over the quarter-chord line near the wing tip (Fig. 7 (c) and (d)). Results show that in the range of angles of attack under experiments, there is no sign of a spanwise-pressure-peak drop, which means that the core of the vortex is successively close to the 40DS wing surface; however, as it is illustrated in Fig. 8, the curve slope of increasing the value of spanwise $C_{p,\min}$ decreases, when increasing the AOA from 8° to 14°. Moreover, like the 23DS wing, with an increasing AOA from 10° to 12°, a sudden pressure drop near the tip of the 40DS wing shows an incipient stall region due to the vortex breakdown, which moves toward the wing root when increasing the angle of attack (Fig. 7(d)).

### 3.2.2. *Effect of increasing sweep angle on spanwise $C_p$*

Fig. 9 shows the effect of increasing the sweep angle on the spanwise pressure distribution at a 2° angle of attack. As it is shown, with an increasing sweep angle, a longitudinal shift in the pressure distribution curve can be observed, which represents a weaker suction force over the quarter-chord line of the 40DS wing. Furthermore, it is clearly seen that as the sweep angle increases, the curve slope of the spanwise $C_p$ decreases.

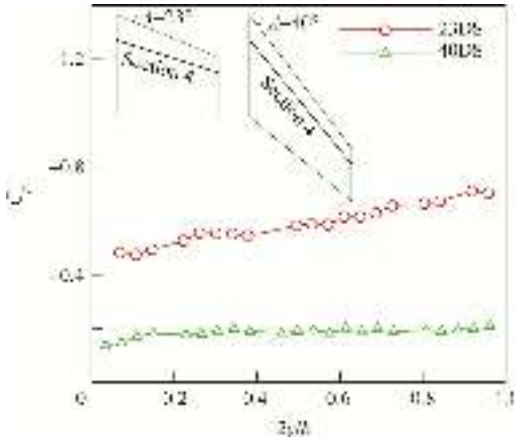

**Fig. 9** Effect of sweep angle on spanwise pressure distribution at $\alpha = 2°$.

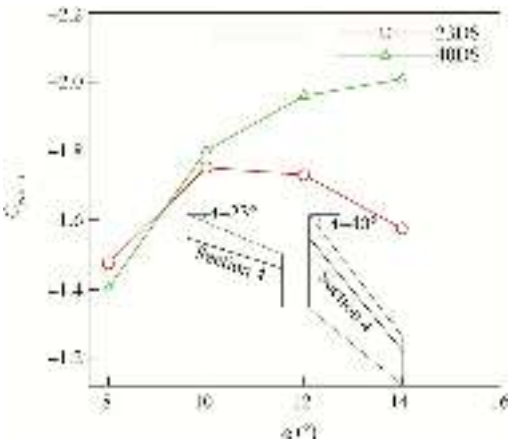

**Fig. 10** Variation of spanwise $C_{p,\min}$.

The results suggest that at a specific AOA, as the wing sweep angle increases, the region covered by the vortex generated on the quarter-chord line near the wing tip decreases in size. As can be seen in Fig. 7(b) and (d), at an AOA of 8°, this area of low pressure decreases from $0.54 < 2y/b < 0.97$ for the 23DS wing to $0.54 < 2y/b < 0.74$ for the 40DS wing.

Fig. 10 illustrates the effects of the AOA and increasing the wing sweep angle on the minimum value of the spanwise pressure distribution. As it can be seen in the figure, at an 8° AOA, $|C_{p,\min}|$ decreases when increasing the sweep angle from 23° to 40°. In other words, at an 8° angle of attack, with an increasing sweep angle, the strength of the vortex formed on the quarter-chord line diminishes. However, it is found that with increasing the AOA to higher values, the magnitude of spanwise $C_{p,\min}$ over the 23DS wing decreases when compared to that of the 40DS wing (Fig. 10). As it is shown, for angles of attack of 12° and 14°, the values of spanwise $C_{p,\min}$ for the wings go in opposite directions; in other words, the vortex formed on the quarter-chord line of the 23DS wing weakens in strength, and the magnitude of its $C_{p,\min}$ drops. On the other hand, the vortex formed on the 40°-sweep wing quarter-chord line gets stronger, increasing $|C_{p,\min.}|$. Although in the range of AOAs under experiments, there is no sign of a sudden drop in spanwise $C_{p,\min}$ for the 40DS wing, it can be predicted that the same process will take place at a higher AOA.

Results show that at a specific angle of attack, increasing the sweep angle results in generating a stronger vortex on the quarter-chord line, which has lower sensitivity to angle of attack variations. In other words, as the sweep angle increases, the vortex remains attached to the wing surface for higher angles of attack, causing vortex breakdown and Sectional stall to occur at higher angles of attack.

### 3.3. *Effect of end plate on chordwise $C_p$*

Figs. 11 and 12 show the results of this investigation (pressure distribution over two swept WWE) and those of[19] (pressure distribution over two swept WOE) at angles of attack of 0°, 2°, 4°, 6°, and 8°. In addition, for more accurate deduction, corresponding streamline tracks over the surfaces of the wings are shown in these figures.

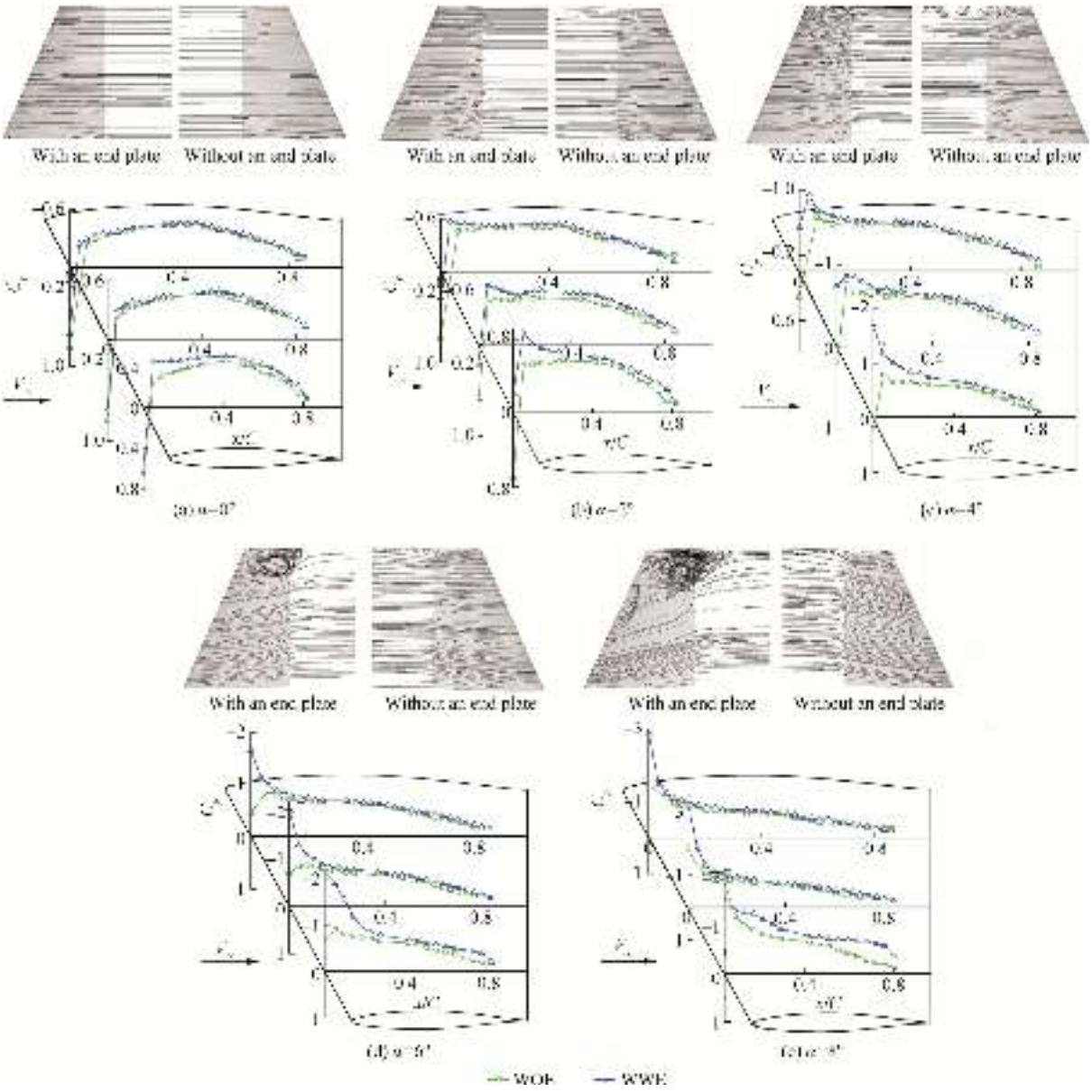


**Fig. 11** Comparison of chordwise $C_p$ for $\Lambda = 23°$.

A comparison of the results shows that in the case of the 23DS wing, at an AOA of 0°, the end plate has almost no effect on the chordwise $C_p$, and the predicted data are in very good agreement with those of[19]; however, the small difference between the two pressure data in the outboard station is within the measurement accuracy range. Moreover, comparing the CFD results of WWE to those of WOE in Fig. 12(a) shows no remarkable difference in streamline traces on the two wing surfaces. As the AOA increases to 4°, data obtained in this investigation present a larger $|C_p|$ near the LE of the chordwise sections than that in the case of WOE. However, the qualitative features of the pressure distributions remain the same as the end plate interference is included (Fig. 11(b)).

The end plate causes a blockage effect on the flow and additional viscous effects, especially near the end plate[24]. It should be pointed out that the use of an end plate which acts as a barrier to the spanwise flow along the outboard portion of a wing and therefore eliminates generation of wing tip vortices, causes the streamlines in the neighborhood of a model to curve as they pass over the wing surface. Moreover, near the wing tip area, the streamlines curve more sharply near the LE and close to the end plate. These spanwise streamlines encountering the end plate result in forming a vortex-shaped flow on the surface of the end plate. It seems that installing an end plate on the tip of a wing model causes the magnitude of pressure coefficient near the LE of the chordwise sections to increase, especially in the outboard-section pressure distribution, when compared to that of WOE, but as the distance from these regions is increased, the comparison shows good agreement specially in the middle and inner sections of the wing (Fig. 11(b)).

Fig. 11(c) and (d) shows that in the case of WWE, increasing the AOA causes the streamlines curve more sharply. Furthermore, the vortex formed on the surface of the end plate increases in size and moves downstream to the end-plate TE,

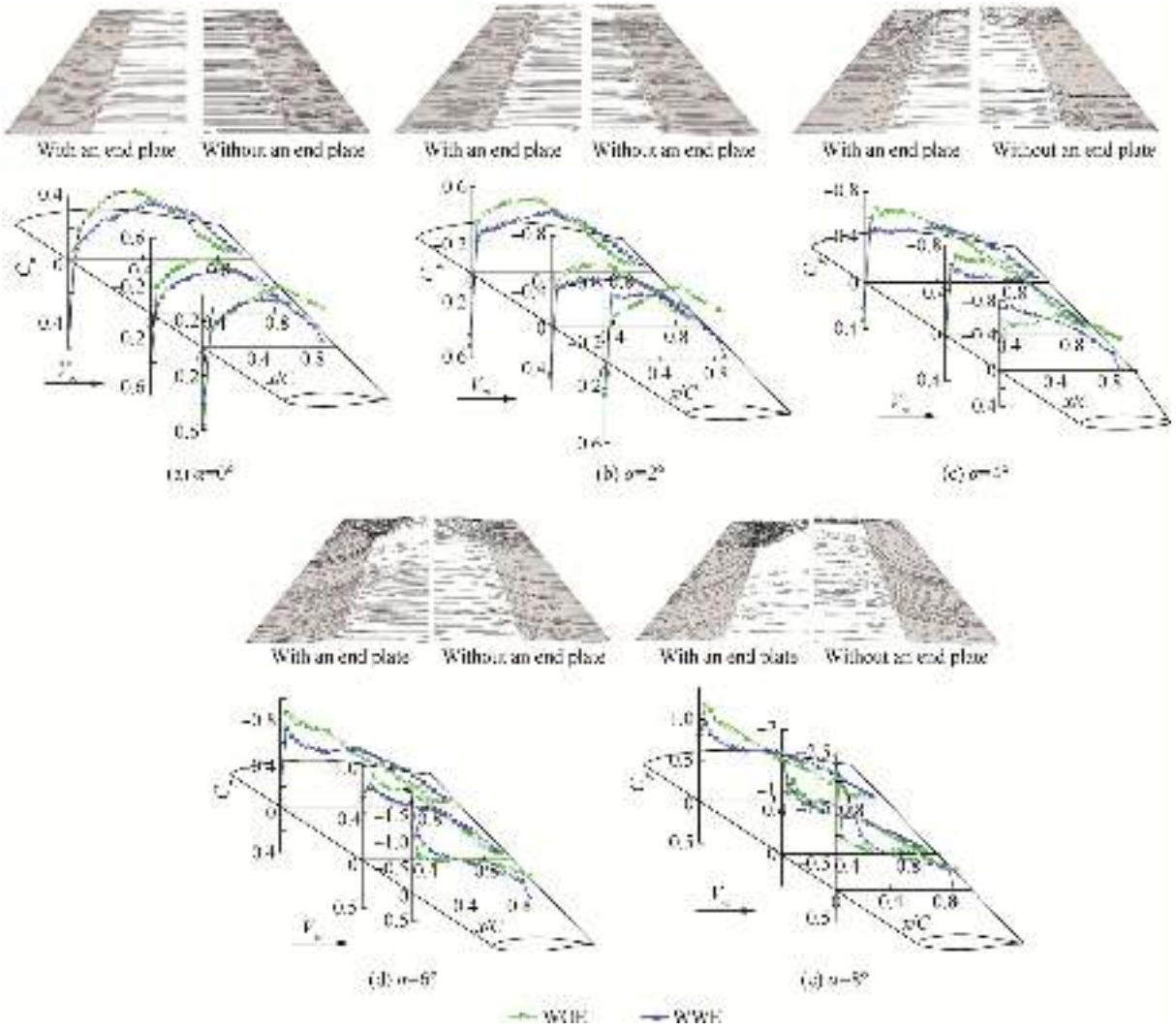


**Fig. 12** Comparison of chordwise $C_p$ for $\Lambda = 40°$.

so that at an 8° AOA, its trace amplitude moves toward the middle section of the wing.

A comparison between Fig. 11(c) and 11(d) shows that as the AOA increases from 6° to 8°, in Sections 1 and 2 pressure distributions, only the areas near the LE are affected by the disturbed flow created on the surface of the end plate. On the contrary, it seems that curving the streamlines more sharply and increasing the size of the end-plate-surface vortex have a greater effect on the wing's outboard-section pressure distribution. As a result, it causes a rapid drop in $C_{p,\min}$ near the outboard-section LE, followed by a lack of pressure recovery toward the TE. As can be seen in Fig. 11(d), in the case of WWE, the pressure data show an area of constant pressure near the LE of Section 3 which covers a region of $0.05 \leqslant x/C \leqslant 0.14$, while in the case of WOE, no indication of a constant pressure area is seen. As previously discussed, the plateau of the pressure distribution curve is a characteristic of a laminar separation bubble, which takes place at lower angles of attack for the case of WWE compared to those of WOE. Moreover, the results show a sudden drop in the magnitude of $C_p$ near the TE of WWE compared to that of WOE.

It is found that by increasing the strength and size of the end-plate-surface vortex, its effect on $C_p$ near the TE increases, which results in a decrease of the airstream velocity near the outboard-section TE. As it is shown in Fig. 11(a)–(d), with an increasing AOA, $|C_p|$ in this area of the wing drops more sharply.

A comparison between Figs. 11 and 12 shows that the end plate has a greater effect on $C_p$ near the LE and TE of the 40DS wing. Moreover, Comparing the CFD results of the two studies solidly confirms that the streamline traces on the 40DS wing surface are affected more greatly by the end plate than in the case of the 23DS wing.

As it is presented in Fig. 12(a), eliminating wing tip vortices causes more gradual acceleration of the flow and more gradual pressure recovery on all chordwise sections of the 40DS wing. This gradual acceleration of the flow from the LE to the minimum pressure point is clearly visible on Sections 1 and 2. Furthermore, the most significant effect of the end plate on pressure recovery occurs in the outboard-Section pressure distribution of the 40DS wing, which is in the vicinity of the vortex formed on the end plate (comparing pressure data of WWE to those of WOE in Fig. 11(a)).

CFD results show that in the case of the 40DS wing with an end plate, increasing the AOA causes the streamlines to curve more sharply toward the wing tip in comparison with those of WOE (Fig. 12(a)–(d)). Furthermore, as the AOA increases, the differences between the pressure results in Sections 1 and 2 remain the same, but in Section 3, the suction force near the LE gets stronger compared to the results of WOE (Fig. 12 (b)–(d)). Moreover, like the case of the 23DS wing with an end plate, the results show a sudden drop in $|C_p|$ near the TE of the 40DS wing with an end plate compared to that of WOE. As discussed before, with an increasing AOA, the end-plate-surface vortex gets stronger, which results in a stronger spanwise flow, thus affecting the airstream velocity near the wing's outboard-Section TE and causing a sudden drop in the pressure distribution. As for the case of the 23DS wing with an end plate, Fig. 12(a)–(d) show that with an increasing AOA, $|C_p|$ drops more sharply in this region of the 40DS wing. According to Ref.[25], the presence of the lateral boundaries around the test-section (the walls of the test-section) produces a lateral constraint to the flow pattern around a body known as solid blocking. For closed throats, solid blocking is the same as an increase in dynamic pressure, increasing all forces and moments at a given angle of attack. Furthermore, the lateral boundaries produce an alteration to the local angle of attack along the span.

It is found that the use of an end plat decreases the test section's cross-sectional area, thus increasing the effect of lateral boundaries. Moreover, according to Ref.[24], the end plate causes a blockage effect on the flow and additional viscous effect, especially near the end plate. These combined effects significantly increase the magnitudes of $C_p$ near the LE of the wing, especially in the outboard Section, and reinforce the spanwise flow over the surface of the wing due to the formation of a vortex-shaped flow on the surface of the end plate. The results show that the use of an end plate to eliminate wing tip vortices have a greater effect on the 40DS wing.

## 4. Conclusions

(1) The results show that localized regions of separation followed by reattachment of the flow in the chordwise-Section pressure distributions occur at angles of attack somewhat below the stall. The region of separation starts near the leading edge of the outboard station (Section 3) and runs inboard and aft in a continuous bubble streak.

(2) As the sweep angle increases, the formation of a laminar separation bubble takes place at higher angles of attack, and at a specified angle of attack, with an increasing sweep angle, the length of the area of constant pressure is decreased. Furthermore, when increasing the sweep angle, the origin of this vortex streak near the leading edge of a wing moves to the outboard Section of the wing.

(3) Increasing the sweep angle causes the stall phenomena on the chordwise Sections of a swept wing to delay.

(4) The results obtained show that with an increasing angle of attack, a vortex forms near the wing tip on the quartet-chord line, which pushes inward from the wing tip to the wing root and increases in size when increasing the angle of attack.

(5) At a specific angle of attack, as the sweep angle increases, the vortex formed on the quarter-chord line gets stronger, further increasing the negative pressure in this region of the wing. In addition, as the sweep angle increases, the vortex remains attached to the wing surface for higher angles of attack, causing vortex breakdown and Sectional stall to delay.

(6) The results show that an end plate causes a blockage effect on the flow and extra viscous effect specifically in the vicinity of the end plate. These joined effects of the end plate significantly result in forming a vortex-shaped flow on the surface of the end plate, and despite our expectations, reinforcement of the spanwise flow over the surface of the wing, thus affecting the pressure distribution, when compared to a wing without an end plate.

## References


1. Nay HO. *Low speed boundary layer and pressure distribution tests on a family of sweep back wings [dissertation]*. Pasadena (CA): California Institute of Technology; 1952.
2. Harper CW, Maki RL. A review of the stall characteristics of swept wings. Moffett Field (CA): NASA Ames Research Center; 1964. Report No.: 64N24822.
3. Anderson BT, Mayer RR. Effects of wing sweep on boundary-layer transition for a smooth F-14A wing at Mach numbers from 0.700 to 0.825. Edwards (CA): NASA Hugh L. Dryden Flight Research Facility; 1990. Report No.: 91N24556.
4. Wing F, Supercritical VC, Powers SG, Webb LD. Flight wing surface pressure and boundary-layer data report from the F-111 smooth variable-camber supercritical mission adaptive wing. Edwards (CA): NASA Dryden Flight Research Center; 1997. Report No.: 91N24556.
5. Soltani MR, Ghorbanian K, Masdari M. Investigation of the pressure distribution and transition point over a swept wing. *Sci Iran* 2011;**18**(6):1277–86.
6. Yen SC, Hsu CM. Investigation on vortex shedding of a swept-back wing. *Exp Therm Fluid Sci* 2007;**31**(8):849–55.
7. Houghton EL, Carpenter PW. *Aerodynamics for engineering students*. 5th ed. Oxford: Butterworth-Heinemann; 2003. p. 522–3.
8. Giuni M, Benard E, Green RB. SPIV experiments on wing trailing vortices. *Engineering graduate school conference*; 2010.
9. Spalart PR. Airplane trailing vortices. *Annu Rev Fluid Mech* 1998;**30**(1):107–38.
10. Sohn MH, Chang JW. Visualization and PIV study of wingtip vortices for three different tip configurations. *Aerosp Sci Technol* 2012;**16**(1):40–6.
11. Fink MP, Lastinger JL. Aerodynamic characteristics of low-aspect-ratio wings in close proximity to the ground. Hampton (VA): NASA Langley Research Center; 1961. Report No.: NASA-TN-D-926, L-1367.
12. Carter AW. Effect of ground proximity on the aerodynamic characteristics of aspect-ratio-1 airfoils with and without end plate. Hampton (VA): NASA Langley Research Center; 1961. Report No.: NASA-TN-D-970, L-1693.
13. Lee J. Influence of end plate on aerodynamic characteristics of low-aspect-ratio wing in ground effect. *J Mech Sci Technol* 2008;**22**(12):2578–89.
14. Boutilier MSH, Yarusevych S. Effect of end plates and blockage on a low Reynolds number airfoil experiment. *41st AIAA fluid dynamics conference and exhibit*. Reston: AIAA; 2011.
15. Alam MM, Zhou Y, Yang HX. The ultra-low Reynolds number airfoil wake. *Exp Fluids* 2010;**48**(1):81–103.

16. Lee T, Gerontakos P. Investigation of flow over an oscillating airfoil. *J Fluid Mech* 2004;**512**:313–41.
17. Pelletier A, Mueller TJ. Low Reynolds number aerodynamics of low-Aspect-Ratio, thin/flat/cambered-plate wings. *J Aircraft* 2000;**37**(5):825–32.
18. Pelletier A, Mueller TJ. Effect of endplates on two-dimensional airfoil testing at low Reynolds numbers. *J Aircraft* 2001;**38**(6):1056–9.
19. Soltani MR, Masdari M, Seidjafari M, Rasi F. Experimental study of the flow field over two swept wings. *13th annual and 2nd international fluid dynamics conference*; 2010.
20. Howard RM. *Principles of random signal analysis and low noise design*. 1st ed. Australia: John Wiley & Sons Inc.; 2002. p. 76–8.
21. Davis RL, Carter JE. Analysis of transitional separation bubble on infinite swept wing. *AIAA J* 1987;**25**(3):421–8.
22. Lee S. *Effect of supercooled large-droplet icing on airfoil aerodynamics [dissertation]*. Champaign (IL): University of Illinois; 2001.
23. White EB, Saric WS, Gladden RD, Gabet PM. Stage of swept wing transition. *39th aerospace sciences meeting & exhibit*. Reston: AIAA; 2001.
24. Jung JH, Kim MJ, Yoon HS, Hung PA, Chun HH, Park DW. Endplate effect on aerodynamic characteristics of three dimensional wings in close free surface proximity. *Int J Nav Arch Ocean* 2012;**4**(4):477–87.
25. Rathakrishnan E. *Instrumentation, measurements and experiments in fluids*. 1st ed. New York: CRC Press; 2007. p. 141–2.